Shaped natural and synthetic zeolites for CO_2 capture in a wide temperature range

Margherita Cavallo [a], Melodj Dosa [b], Natale G. Porcaro [a], Francesca Bonino [a], Marco Piumetti [b,*], Valentina Crocellà [a,*]

[a] Department of Chemistry, NIS and INSTM Reference Centers, Università di Torino, Turin 10135, Italy
[b] Department of Applied Science and Technology, Politecnico di Torino, Turin 10129, Italy

A B S T R A C T

The CO_2 adsorption performances of a Linde-Type A (LTA) zeolite and a natural Clinoptilolite (Clino) zeolite, both in shaped form, were investigated as such or after an ion-exchange procedure and compared to assess their potential application as solid adsorbents for Carbon Capture and Storage (CCS). The samples were characterized following a multi-technique approach. Their structural and textural properties were evaluated to investigate the accessibility of the different ions present inside the microporous structure and the strength of their interaction with the adsorbates. The CO_2 adsorption tests were carried out performing pure CO_2 adsorption/desorption isotherms and dynamic breakthrough measurements in a wide range of temperature (298–423 K). The ion-exchange enhanced the adsorption capacity of the synthetic zeolite, while no significant increment in the CO_2 adsorption performances is observed for the natural one. Nonetheless, the CO_2 adsorption reversibility is affected by the cation exchange process in both synthetic and natural zeolites. The CO_2 adsorption capacities of LTA zeolites are higher at lower temperatures, whereas the CO_2 adsorption performances of natural Clino are interesting also at medium-high temperature, being the most performant material at 423 K. By performing IR experiments with specific probe molecules, the presence of a consistent number of Fe^{2+} ions in the framework of natural Clino, responsible for the capacity of this material to strongly interact with CO_2 also at medium-high temperatures, was proved. The peculiar adsorption behavior of natural Clino, its low cost and availability in shaped form are some of the essential features for its possible implementation in real CCS technologies.

1. Introduction

Carbon dioxide (CO_2) is naturally occurring in the Earth's carbon cycle, and it is exchanged among plants, animals, soils and oceans in the biosphere. However, the CO_2 amount in the atmosphere has significantly increased during the last decades, due to the human activities that have irreversibly altered the atmospheric CO_2 concentration, by modifying the capture capacity of forests and soils and by directly releasing huge amount of CO_2. The combustion of fossil fuels (i.e., coal, oil, and natural gas) is the main responsible of the CO_2 emissions in the atmosphere. In particular, the following emission percentages by field were reported: 35 % transportation, 31 % electricity production, 16 % industry, 10 % residential and commercial and 8 % non-fossil fuel combustion [1]. In 2019, the amount of CO_2 in the atmosphere was about 80 % of all greenhouse gasses emissions, while the contribution of the other stood at 10 % for methane (CH_4), 7 % for nitrous oxide (NO_x) and 3 % for

fluorinated gases [1]. Due to the huge amount of CO_2 emissions, this molecule remains the major responsible for the greenhouse effect, even if its global warming potential is lower than the one estimated for other GHGs [1,2]. In the last decades, several strategies have been developed to decrease the amount of CO_2 in the atmosphere. The attention of the scientific community has mainly focused on the development of technologies aimed at reducing the emissions of CO_2 deriving from electricity and industrial productions, which account together for about 47 % of the total emissions. Nowadays, the main Carbon Capture and Storage (CCS) technologies employed in the post-combustion CO_2 capture are chemical and physical absorption, adsorption-based solid materials, cryogenics methods, membranes, microbial/Algal systems and solvent scrubbing [3–7]. The CO_2 capture by solid adsorbents has gained particular interest thanks to several advantages, as low energy costs, mild regeneration conditions and low volatility of the captured CO_2 [7]. Among the possible adsorbents for the CO_2 capture, zeolites possess

some interesting features due to their textural, structural and chemical properties, as far as for their high cation exchange potential and polarity properties [7–15]. For this reason different synthetic and natural zeolites have been widely studied in academia for CO_2 capture over the years [16].

In this scenario, Clinoptilolite, a natural zeolite, has received interest for CO_2 capture due to the low-cost comparing to commercial (synthetic) zeolites (vide infra), which depends on its chemical composition and geographical origin [17–20]. This natural material, which belongs to the heulandite (HEU) framework-type group, exhibits a $(NaKCa)_4(Al_6Si_{30}O_{72}) \cdot 24H_2O$ unit cell formula and is characterized by two parallel channels (0.30×0.76 nm and 0.33×0.46 nm) connected with a third one (0.26×0.47 nm) [21].

Among the synthetic zeolites, LTA (Lynde-Type A), generally applied as an industrial desiccant, has been recently studied for the adsorption of other molecules, including CO_2 [22,23]. The general formula of this zeolite is $\left| Na^+_{12}(H_2O)_{27} \right|_8 [Al_{12}Si_{12}O_{48}]_8$ and is commonly available with Na^+ as extra-framework cations balancing the negative charge given by the presence of aluminum atoms. The lowest possible Si/Al ratio of this zeolite (Si/Al = 1) leads to a higher cations exchange capacity, with possible positive effects on the CO_2 uptake of the material [24]. In LTA, tetrahedra are organized to form a structure composed by 8 beta cages (sodalite cages) connected each other with cubic structures (d4r), creating a central alpha cage (made by 48 T structures). The dimension of the diameter of the central alpha cage is 1.1 nm, while the external 8-member ring aperture is about 0.4 nm [25].

Both the Clinoptilolite and the LTA zeolites can adsorb CO_2 by Van der Waals forces and the modification of their chemical composition (i. e., by varying the nature of cations present in the framework) may increase the CO_2 adsorption capacity [26]. However, beside the great interest of zeolites as CO_2 adsorbents, for an actual application in the industrial sector, adsorptive flue gases should be dehydrated due to their well-known strong affinity for water. [27].

This aspect affects the energy consumption, increasing the final cost of the entire process. [28,29] For this reason, to be compatible with other established or emerging technologies and to be considered worthy of industrial potential, those adsorbent materials must at least comply with other specific requirements, such as low costs, regeneration capacity, cyclability, selectivity and availability into mm-scale shaped particles.

In the present work, both Clinoptilolite and LTA zeolites were studied in an already shaped form and compared to evaluate their CO_2 adsorption capacity at various temperatures (in the 298–423 K range) to assess their potential application as CCS adsorbents in different capture conditions. Moreover, to possibly enhance their adsorption capacity, both samples were ion-exchanged with different cations. The materials were deeply characterized by using different complementary techniques and their CO_2 capture capacity were investigated in both static ideal and flow conditions by collecting CO_2 adsorption experiments with pure CO_2 and under a N_2/CO_2 flow.

2. Experimental methods

2.1. Materials preparation

The natural zeolite Clinoptilolite (herein labeled as "Clino") was provided by Zeolado (Greece), while the synthetic LTA (hereafter referred to as "NaLTA") was purchased in sodic form from Sigma Aldrich. Usually for research purposes, the samples are supplied in powder form, whereas for practical and industrial applications the use of already shaped materials into mm-scale particles is required [30]. For this reason, a LTA in spherical beads (ø 3–5 mm) and a Clino in natural rock fragments (ø 0.15 mm) were used in the present work.

Due to its natural origin, Clino contains many different cations (Fe, K, Ca, Na, Mg). To homogenize its composition and discriminate the effect of different cations, NaClino and CaClino were prepared starting from the pristine Clino. Similarly, CaLTA was generated from pristine NaLTA, using a similar ion-exchange procedure as graphically described in Scheme1.

The difference in the two ion-exchange procedures consists in a previous de-cationization process needed for natural Clino. The cations substitution in this framework is usually hard if compared to other types of zeolites, due to the stronger interaction of Clino cations with the structure [31,32]. In order to increase their exchange capacity, a previous substitution with NH_4^+ ions is commonly performed, exploiting the high selectivity of Clino for these cations [33].

The exchange method employed for Clino was adapted from the procedure reported by Valdés et al. [33]. A preliminary washing procedure was performed on the starting Clino: the material was washed in ultra-pure water at room temperature under stirring for 10 min, centrifuged and oven-dried at 348 K for 12 h. The washed Clino was first exchanged with NH_4^+ ions by immersing for 2 h the sample in a 0.1 M solution of $(NH_4)_2SO_4$ (30 mL solution/g sample) under stirring at 363 K. The sample was washed by replacing the solution with ultra-pure water and stirred at 363 K overnight. This procedure was repeated twice to improve the exchange ratio and finally the sample was oven-dried at 398 K overnight. After this step, the NH_4^+ ions were exchanged with Na^+ and Ca^{2+} to obtain a fully exchanged Na-Clino (NaClino) and Ca-Clino (CaClino) respectively. The sample in ammonic form was immersed for 18 h in a 0.5 M solution of $NaNO_3$ (for NaClino) or $Ca(NO_3)_2$ (for CaClino) under stirring at 333 K (20 mL solution/g sample). The procedure was repeated a second time by replacing the solution with a fresh one. The sample was eventually dried at 373 K overnight and stored in a desiccator until further use.

In contrast to Clino, the NaLTA can be easily exchanged with a simple ion exchange procedure [34]. Therefore, an LTA sample exchanged with Ca^{2+} ions (CaLTA) was prepared by immersing the original NaLTA sample in a 0.5 M solution of $Ca(NO_3)_2$ (20 mL solution/g sample), following the same conditions used for CaClino. Also in this case, the procedure was repeated twice.

2.2. Characterization methods

The EDX analysis were performed on a FESEM TESCAN S9000G. The voltage used for electron acceleration is 15 kV and the probe current 300 pA, the software AZTEC was used for the microanalysis.

FT-IR spectroscopy was employed to follow the CO adsorption at 77 K by using a Bruker Invenio spectrophotometer equipped with a MCT (mercury cadmium tellurium) cryo-detector. All the spectra were collected in the 4000–650 cm^{-1} spectral rage with a resolution of 2 cm^{-1} and an average of 32 scans. Before the analysis all the samples, in form of self-supported pellets protected by a gold envelope, were inserted in a special home-made quartz cell and activated in vacuum at 673 K for 4 h. Then, they were cooled down to Room Temperature (RT) and approximately 60 mbar of CO were dosed to the sample. The cell was cooled down with liquid nitrogen until reaching a nominal temperature of 77 K, at which the interaction of CO with the cationic acid sites of the zeolite are well visible. Finally, different spectra were collected during gas expansions until all CO was desorbed.

The powder X-ray diffractograms of the materials were collected on a PANalytical X'Pert diffractometer using Cu Kα radiation and a power of 45 kV 40 mA in Capillary configuration (2θ range = 5–65°).

Volumetric measurements were performed by means of a Micromeritics ASAP2020 sorption analyser, by collecting adsorption/ desorption isotherms of both N_2 at 77 K and CO_2 at 273 K up to 1000 mbar. For CO_2 adsorption, the temperature was kept constant thanks to a special home-made patented apparatus coupled with the Micromeritics ASAP 2020 volumetric instrument, consisting of a glass buret inserted in a concentric jacket, in which a coolant or heating fluid circulates through a JULABO CD-200F [35]. The system ensures precise temperature control during the measurement in terms of homogeneity
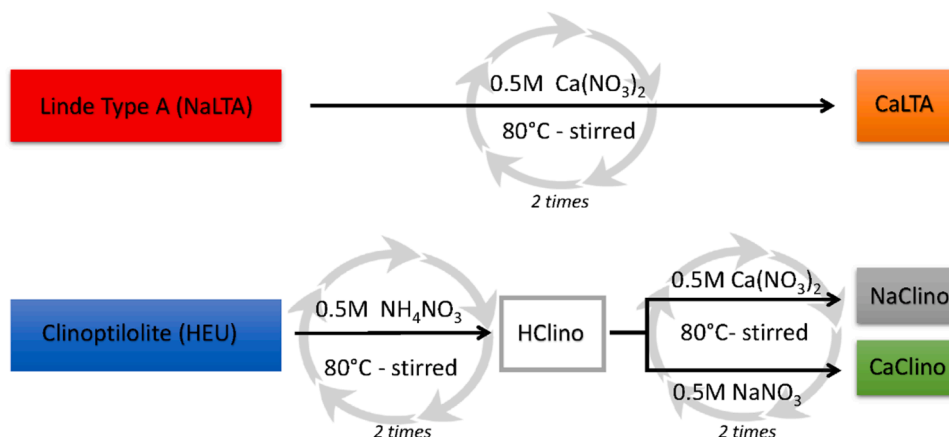
Scheme 1. Schematic representation of ion-exchange procedure for the two samples.

and stability over time, allowing isotherms collection with a very low temperature resolution. Before the measurement, the samples were activated at 673 K for 4 h in vacuum.

The CO_2 adsorption/desorption isotherms were measured at other four different temperatures (298, 333, 363 and 423 K) using the same volumetric set-up and following the same activation procedure. The specific surface area was determined by both N_2 and CO_2 adsorption isotherms, applying the Brunauer–Emmett–Teller (BET) equation in the $0.05 < p/p_0 < 0.3$ and $0.003 < p/p_0 < 0.03$ range respectively.

An evaluation of the isosteric heat of adsorption was also performed by applying the Clausius-Clapeyron equation to the isotherms measured at the first three temperatures (298, 333, 363 K) [36]:

$$Q_{st} = RT^2 \left(\frac{\partial lnp}{\partial T} \right)_q \tag{1}$$

Different isosteric curves can be obtained plotting the natural logarithm of the pressure at constant loading as a function of 1/T. Multiplying the slope of this curve by the gas constant the isosteric heat for different quantities adsorbed was obtained [37]. Data elaboration was performed by using the Micromeritics' data analysis software (Micro-Active version 5.02.01).

Breakthrough CO_2 adsorption tests were performed in an experimental set-up characterized by the following equipment: a quartz-U reactor (inner diameter 1 cm, height 3 cm) with a fixed bed, a furnace and a paramagnetic gas analyzer (Emerson XStream X2GP). In this set-up, the adsorbent material (300 mg) was placed into the quartz-U reactor. The reactor was positioned into the furnace and connected to the mass-flow controllers. A K-type thermocouple, placed in the quartz-U reactor chamber on the top of the adsorbent material (at around 1 mm distance), was used for the temperature control. The flow-out from the reactor was monitored by the gas analyzer every 10 s, monitoring the CO_2 volume fraction (ppm). Before the adsorption tests, a pretreatment was carried out to eliminate impurities on the adsorbent material (i.e., carbonates and humidity). The pretreatment was performed by using N_2 (total flow = 40 mL min^{-1}) at 673 K for 2 h. Then, the temperature was cooled down and the adsorption tests were performed: the total flow was 40 mL min^{-1} comprised by 10 vol% CO_2 volume balanced with N_2. The temperatures chosen for the CO_2 adsorption tests were 298, 333, 363 and 423 K, according to the volumetric measurements. In each adsorption test, the CO_2 volume fraction was recorded until the concentration reaches the initial value (10 vol%). The amount of CO_2 was evaluated by the integration of the breakthrough curves, as reported in the Supplementary material.

Furthermore, the adsorption loading capacities of the adsorbent materials were evaluated by the following equation:

$$\alpha_{zeolite} = \frac{n_{CO_{2adsorbed}}}{m_{sorbent}} \tag{2}$$

where:

$n_{CO_{2adsorbed}}$ is the total amount of CO_2 (moles) adsorbed by the material.

$m_{sorbent}$ is the total amount (mass - g) of adsorbent material used for the test.

3. Results and discussions

### 3.1. Physico-chemical characterization

A first proof of the efficacy of the ion-exchange procedure was verified by means of EDX analysis, which provides the elemental composition of the zeolites. Results are summarized in Table 1 for all samples. The resulting values are an average obtained analyzing five points located in different regions of the samples.

The pristine Clino is characterized by the presence of different cations inside the HEU framework, the most abundant being Fe, followed (in order of abundance) by K^+, Ca^{2+}, Mg^{2+}, and Na^+. Fe can be present as Fe^{2+} and Fe^{3+} in different ratio, depending on the geographical origin of the clinoptilolite [38]. In NaClino exchanged sample, Na^+ has the highest atomic and weight percentage, underlining that the ion exchange procedure probably succeeded mainly at the expense of $Fe^{2+/3+}$ and Ca^{2+} cations, leaving small amounts of Mg^{2+} and K^+ inside the framework. Similarly, $Fe^{2+/3+}$, Mg^{2+} and Na^+ were entirely substituted by Ca in CaClino, whereas a small fraction of K^+ ions remain in the zeolite framework. For all the Clino samples the Si/Al ratio is around the theorical value (~5), with a slight increase in the exchanged sample probably due to a partial dealumination [39]. As expected for a synthetic zeolite, in the starting NaLTA sample the main cation present in the zeolite framework is Na^+, with some Ca^{2+} and Mg^{2+} impurities. Na^+ ions are mostly substituted by Ca^{2+} in the CaLTA sample, proving that a milder ion exchange procedure, without a decationization step, is sufficient to replace the cations of the LTA zeolite beads. Both NaLTA and CaLTA exhibit a Si/Al ratio around the theorical value (~ 1), proving that the exchange procedure does not modify the Al content of the sample.

XRD patterns were collected to prove that the crystalline structure of the zeolites was not affected by the ion-exchange procedure. As reported in Fig. 1, Clino, NaClino and CaClino samples exhibit the main reflections of the HEU framework, [40,41] whereas NaLTA and CaLTA samples show the characteristic diffraction pattern of the LTA topology. [42] The broader peaks of Clino sample could be associated with the presence of smaller crystals compared to LTA. Both the zeolites display no changes in the position of the main peaks, confirming that the zeolite structure has been preserved after the ion-exchange process.

Table 1
Elemental composition of the samples obtained by EDX analysis.

Sample	Weight (%)					Atomic (%)					Si/Al atomic ratio
	Fe	*K*	*Na*	*Ca*	*Mg*	*Fe*	*K*	*Na*	*Ca*	*Mg*	
Clino	4.65	2.60	0.25	1.45	0.80	1.75	1.40	0.22	0.76	0.71	4.62
NaClino	–	0.85	2.70	–	0.35	–	0.44	2.38	–	0.29	4.95
CaClino	–	0.70	–	3.50	–	–	0.36	–	1.76	–	4.97
NaLTA	–	–	12.45	0.30	2.10	–	–	10.99	0.29	1.75	1.28
CaLTA	–	–	1.35	13.00	1.55	–	–	1.26	6.92	1.36	1.29
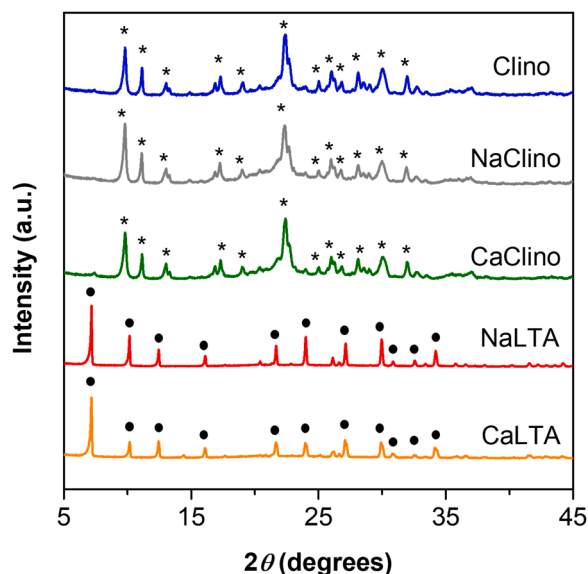
Fig. 1. X-ray diffraction patterns of the starting (Clino and NaLTA) and ion-exchanged (NaClino, CaClino and CaLTA) samples. Asterisks: main reflections of HEU framework. Circles: mail reflections of LTA framework.

The elemental analysis suggests the ion exchange process occurred successfully. The semi-quantitative information about the composition of the samples can be further valorized by performing IR spectroscopy using carbon monoxide (CO) as molecular probe. CO is commonly used in IR spectroscopy in zeolites characterization, for studying the presence of isolated ions located in the structure [43,44]. Indeed, being a weak basic probe and not having steric limitations, CO possesses the subtle ability to discriminate between sites of slightly different acidity located inside the microcavities of the zeolitic structure. Thanks to its Lewis basic character, CO can interact with Lewis acids sites, like cations, forming carbonyl complexes.

This molecular probe has a small dipole moment but a rather high polarizability. Therefore, the stretching frequency of CO adsorbed on alkaline/alkaline earth cations (through the carbon atom) exhibits a hypsochromic shift with respect to the stretching frequency of the free gaseous molecule (2143 cm^{-1}), resulting from polarization and from the consequent increase in the force constant of the C—O bond. The C-bonded carbonyls show an upward shift proportional to the strength of the Lewis acidity of the cations involved in the interaction, allowing the exact determination of the actually accessible ions present in the structure [45,46].

Fig. 2A–F reports the IR spectra of CO adsorbed on the different zeolites, after activation in vacuum at 673 K, in the spectral region of C≡O vibrational modes between 2250 and 2050 cm^{-1}. The spectra of the materials, showing the full mid-IR spectral region before CO contact, are provided in Fig. S1. Concerning the natural Clino (Fig. 2A) the different types of cations present in the sample are responsible for the complex envelope of bands observable at the maximum CO coverage (see blue spectrum). Indeed, as previously pointed out, the composition

of natural zeolites is closely related to their origin, but the major cations present inside the Clinoptilolite framework are usually Fe$^{2+/3+}$, K$^+$, Na$^+$, Ca^{2+} and Mg^{2+}, as confirmed by EDX analysis [47]. For some of them, the interaction with CO causes the appearance of vibrational bands in the same spectral range, making the assignment of the different IR signals not straightforward. For pristine Clino, five main components can be distinguished in the 2250–2050 cm^{-1} spectral range at 2197, 2183, 2163, 2155 and 2148 cm^{-1}, with a different spectral behavior by varying the CO coverage. The signals at 2197 and 2183 cm^{-1} are the most stable (i.e. less reversible upon CO outgassing) and could be associated to the interaction of CO with Fe^{2+} and with Ca^{2+} cations respectively [48–51]. The assignment of these bands is not unambiguous due to the existence in the same spectral region of the signals generated by CO adsorption on Mg^{2+} ions [52]. However, the high amount of Fe detected by EDX together with the intensity and persistence of the 2197 cm^{-1} band, would be inclined to assign this component to Fe^{2+} ions. The less persistent signal at 2163 cm^{-1} can be ascribed, also considering the elemental analysis obtained by EDX, to the CO-K$^+$ adducts, nevertheless a possible overlap of signals can occur also in the present case, because the components due to the interaction of CO with Na$^+$ ions fall in the same spectral range (2162–2172 cm^{-1}) [53,54]. The band with apparent maximum at 2155 cm^{-1}, which readily disappears upon CO outgassing, is probably due to the interaction of CO with the OH groups of the zeolite, as testified by the IR spectra reported in the extended IR region of Fig. S1A where a clear perturbation of the OH stretching modes between 3800 and 3500 cm^{-1} is evident when CO interacts with the sample. The band at 2148 cm^{-1}, visible in the spectra at high CO coverage as a shoulder, reveals its actual profile and persistent nature just upon CO desorption: it should be ascribed to CO molecules bridging two K$^+$ cations. Finally, the weak and labile band located at around 2130 cm^{-1} is due to a small fraction of liquid-like CO phase, which forms inside the zeolite micropores [55].

The IR spectra of Clino sample exchanged with Na$^+$ ions (NaClino), collected at 77 K are reported in Fig. 2B. The envelope of bands generated by the CO interaction with the sample is definitely less complex compared to pristine Clino, with only two intense and well-defined components at 2163 and 2175 cm^{-1} exhibiting a similar behavior upon CO outgassing. These bands can be attributed to CO-K$^+$ and CO-Na$^+$ adducts respectively. At low CO coverage, a weak band at 2197 cm^{-1}, ascribed to Mg^{2+} ions, is also visible upon magnification. The species detected by CO are perfectly in agreement with the results of the EDX analysis, highlighting the difficulty to totally exchange the K$^+$ ions with Na$^+$ cations in the natural zeolite. [56].

The adsorption of CO onto CaClino (Fig. 2C) result in the formation, at the highest CO coverages, of an intense signal at 2183 cm^{-1} which readily undergoes an upward shift at ~ 2200 cm^{-1} upon outgassing. This behavior is due to the gradual conversion of Ca^{2+}(CO)$_2$ dicarbonyls into monocarbonyls species [56]. At high CO coverage, a labile shoulder at around 2170 cm^{-1} is probably ascribed to the presence of residual K$^+$ ions, as already proved by the EDX analysis. In the ion exchanged CaClino sample, the band of liquid-like CO at 2139 cm^{-1} is more evident than in the other Clino samples, due probably to a larger fraction of void volume inside the zeolite microchannels, left by the exchange of monovalent ions with divalent ones.

A comparison of IR spectra of Clino, NaClino and CaClino are
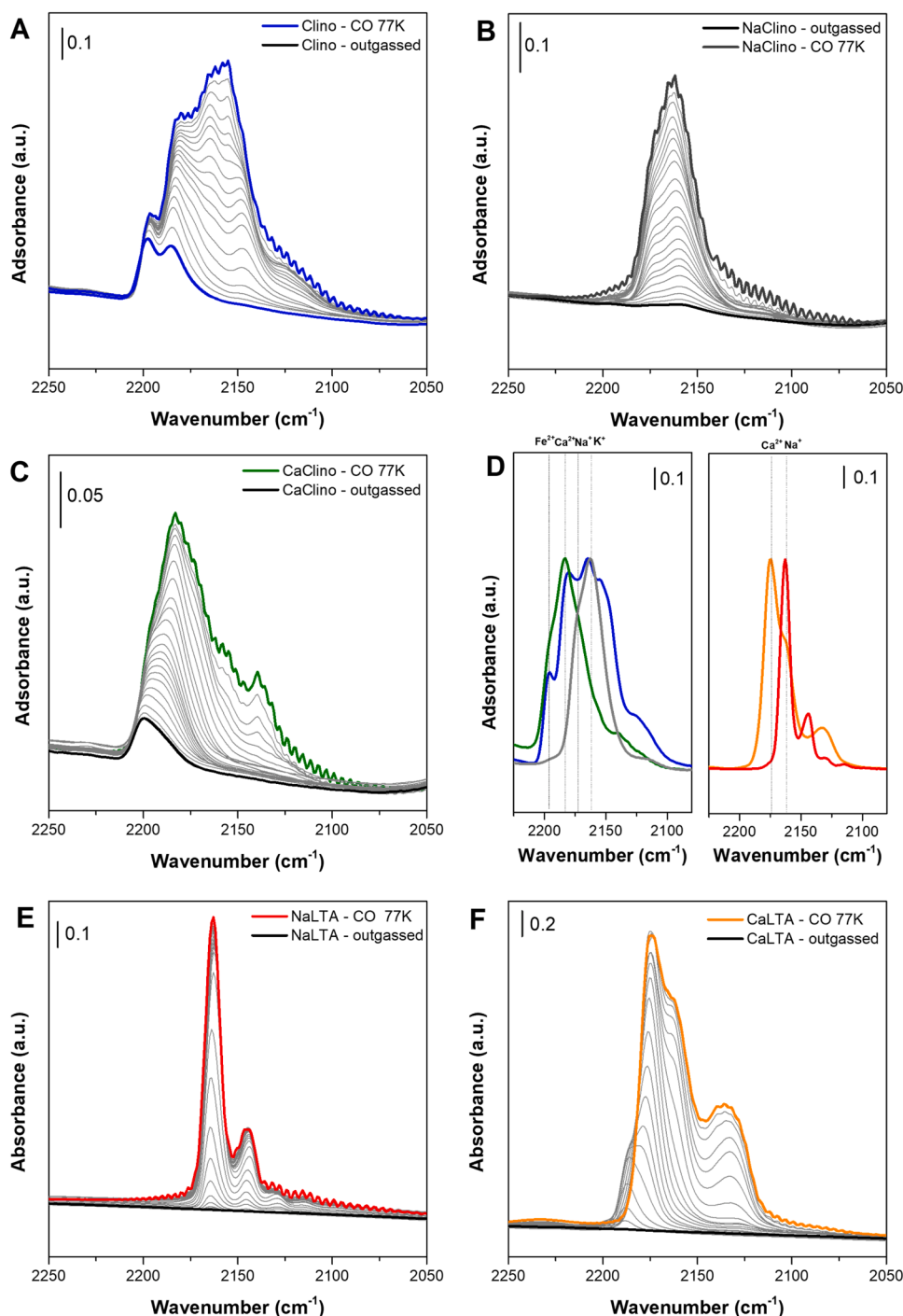
Fig. 2. IR spectra of CO adsorption at 77 K on activated samples, recorded at different CO coverages and reported in the CO vibrational modes region: A) Clino, B) NaClino C) CaClino, E) NaLTA and F) CaLTA. D) Comparison of normalized spectra of LTA (right) and Clino (left) samples at the same CO pressure (0.1 and 0.5 mbar respectively). Colored spectra: maximum CO coverage (60 mbar). Light grey spectra: decreasing pressure steps. Black spectra: outgassing in vacuum until 10^{-3} mbar. Dotted lines represent the position of the main cations expected in the different ion-exchanged samples.

reported in Fig. 2D (left side) at the same CO coverage, to better appreciate the spectroscopic differences among the various samples. The spectrum of pristine Clino (blue curve) exhibits a complex profile, testifying the formation of different adducts with CO, whereas the predominance of Na^+ and Ca^{2+} cations is clear in NaClino and CaClino spectra (gray and green curves respectively). In both cases, the CO-K^+ adducts are also evident, proving the difficulty in totally replacing the K^+ monovalent ions, whereas the signal ascribable to Fe^{2+} cations is totally absent, confirming the complete exchange of this cations with Na^+ or Ca^{2+}.

The interaction of CO with the LTA zeolite is reported in Figs. 2E and 2F. Spectra of CO adsorption at 77 K on the commercial LTA sample in sodic form (NaLTA) are reported in Fig. 2E. The CO stretching region

displays the presence of two well-resolved signals. The sharp band at 2163 cm^{-1} is assigned to Na^+-CO adducts, whereas the component at 2145 cm^{-1} is due to the C-O stretching mode of CO molecules bridging two Na^+ ions [57]. Finally, the weak band at around 2130 cm^{-1} is due to a small fraction of liquid-like CO phase.

The interaction of CO with CaLTA (Fig. 2F) shows a band at ~ 2174 cm^{-1} which exhibits an upward shift till ~ 2186 cm^{-1} upon outgassing. According to Montanari et al. [58] the signal at 2174 cm^{-1} can be associated to $Ca^{2+}(CO)_2$ dicarbonyls (less energetically stable) which decompose during outgassing to give $Ca^{2+}CO$ monocarbonyls, more energetically stable and shifted at higher wavenumbers. The component located at 2163 cm^{-1}, which readily disappears by decreasing CO pressure, can be assigned to Na^+ carbonyls, in accordance

with the atomic percentages of the EDX elemental analysis (Table 1). The broad and labile band detectable at ~ 2135 cm^{-1} can be confidently associated to the liquid-like CO. It is worth noting that the signal associated to liquid like CO is particularly intense for CaLTA, as already observed for the CaClino sample. This consideration suggests the presence of a lower limitation in the probe molecule diffusion and adsorption inside the CaLTA cages.

The comparison between NaLTA and CaLTA spectra (Fig. 2D right side), at the same CO coverage, points out the successful exchange procedure in the Ca containing sample.

Considering the results of CO adsorption, it is clear that the ion exchange process has modified the relative content of the cations present in both Clino and LTA frameworks (enhancing the presence of the desired ion), even if, as already highlighted by the EDX analysis, the ion exchange is not complete. This behavior is particularly evident for the natural zeolite, containing a significant fraction of K$^+$ ions.

More in general, the detailed study of CO adsorption fully confirmed the results obtained by EDX analysis and, at the same time, allowed the evaluation of the actual accessibility of the cations present inside the zeolitic framework to a small molecule in the gas phase.

The Specific Surface Area (SSA) of the samples, computed applying the BET equation, are reported in Table 2. It is well known that the narrow micropores of a type A zeolite cannot be assessed by N$_2$ adsorption at 77 K due to its slow kinetic of diffusion at cryogenic temperature [59]. Indeed, the restricted diffusion prevents nitrogen molecules from entering the microcavities of this zeolite, hindered by the presence of a huge number of cations. However, N$_2$ adsorption at 77 K was anyhow carried out on both LTA and Clino series to evaluate the effect of the presence of different cations inside the microporous cavities on the textural properties of the materials [60,61]. The adsorption/desorption isotherms of N$_2$ at 77 K are reported in Fig. S2 of the Supplementary material. Among the different substituted zeolites, the CaLTA sample exhibits a reasonable SSA computed with N$_2$ at low temperature. In LTA framework, the substitution of Na$^+$ ions located near the aperture of the pores with Ca^{2+} cations, having a lower ionic radius, facilitates the diffusion of N$_2$ inside the microporous structure [62,63]. The high content of liquid like CO phase detected during IR adsorption experiments in the CaLTA compared to NaLTA sample (Fig. 2F) further testifies the presence of a larger fraction of void volume accessible to the probe molecule. N$_2$ adsorption at 77 K in the HEU framework exhibits the same diffusional problems observed for the synthetic zeolite (see N$_2$ isotherms reported in Fig. S2 and SSA values listed in Table 2), due to the presence of a huge number of cations needed for compensating the negative charge induced by the high Al content of this zeolite. In contrast to the synthetic zeolite, the Ca-exchanged Clino sample (CaClino) did not show an increment in SSA, probably due to the different location of the ions inside the Clino framework and to the presence of different residual cations hindering the pores filling. The results obtained with N$_2$ for the Clino samples are compatible with those reported in the literature, however small variations could be due to the different origin of this natural zeolite [64].

Table 2
BET specific surface area of Clino, NaClino, CaClino, NaLTA and CaLTA derived from N$_2$ and CO$_2$ adsorption isotherms at 77 and 273 K respectively.

Sample	N$_2$ adsorption, 77 K S$_{BET}$ (m^2 g^{-1})[a]	CO$_2$ adsorption, 273 K S$_{BET}$ (m^2 g^{-1})[b]
Clino	22 ± 1	240 ± 1
NaClino	43 ± 1	233 ± 1
CaClino	48 ± 1	201 ± 2
NaLTA	26 ± 1	378 ± 2
CaLTA	438 ± 9	447 ± 1

[a] Computed applying the BET equation to the N$_2$ adsorption isotherm at 77 K in the 0.05–0.3 p/p$_0$ range.
[b] Computed applying the BET equation to the CO$_2$ adsorption isotherm at 273 K in the 0.003–0.03 p/p$_0$ range.

A valuable adsorptive for a correct assessment of the porosity of ultramicroporous materials is CO$_2$, which is usually measured at 273 K (see CO$_2$ isotherms reported in Fig. S3 and SSA values listed in Table 2) [65]. Even if the CO$_2$, with its large quadrupole moment could be responsible for specific interactions with the cations of the zeolites, this measurement can still be useful to evaluate the specific surface area of materials which cannot be assessed by nitrogen or argon adsorption at cryogenic temperature, as reported elsewhere [66–69]. In this case, the synergistic effect of its slightly lower kinetic diameter (3.3 Å) [70] and the higher temperature of adsorption results in an easier entrance and diffusion into the ultramicropores of the zeolite [71]. Indeed, a steep increment in SSA value can be observed in all the samples previously unable to adsorb N$_2$ molecules at 77 K. The difference in SSA values between CO$_2$ and N$_2$ displayed by all the samples (except for CaLTA) suggests a great selectivity of those materials toward CO$_2$. The specific surface area of Clino samples computed by CO$_2$ is around 200–240 m^2/g: variations among samples are due to the different cations population. The SSA values computed for LTA samples in spherical beads are definitely higher compared to Clino series. The specific surface area of CaLTA obtained by CO$_2$ adsorption at 273 K (447 m^2/g) is totally comparable to the value computed by N$_2$ adsorption at 77 K (438 m^2/g). Moreover, the SSA of this sample is higher compared to the pristine NaLTA beads (378 m^2/g) due to the lower concentration of divalent Ca^{2+} cations required in the zeolite framework to compensate the negative charge and, at the same time, to their smaller ionic radius.

3.2. Evaluation of CO$_2$ adsorption capacity: volumetric measurements

The pure CO$_2$ adsorption capacity was evaluated for all samples by collecting isotherms at different temperatures (298, 333, 363, 423 K), until 1100 mbar, as reported in Fig. 3A, D, 3G and 3L. Their adsorption capacities at 100 and 1000 mbar were reported in the respective histograms (middle and right frames of Fig. 3) and in Table S1 (Section S4 of SI) to better highlight the adsorption trend at different temperatures. The pressure of 1000 mbar was chosen to evaluate the adsorption capacity at atmospheric pressure, while 100 mbar is the CO$_2$ pressure employed in breakthrough curves since the CO$_2$ adsorption tests were performed with 10 vol% CO$_2$ (total pressure during the tests = 1000 mbar, partial CO$_2$ pressure during the tests = 100 mbar). As pointed out by the histograms, despite the absolute values, the CO$_2$ uptake capacity of the samples at 298 and 333 K has the same trend at the two selected pressures, with the LTA zeolite prevailing over the Clino. In contrast, a different adsorption trend between the two pressures can be detected at 363 K, becoming even more evident at 423 K.

For all the samples, the isotherms in Figs. 3A, 3D, 3G and 3L exhibit a general predictable decrease of the CO$_2$ uptake by increasing the temperature. At 298, 333 and 363 K, CaLTA seems to have the highest CO$_2$ adsorption capacity at high pressures (orange curves) followed by NaLTA (red curves). At 363 K, the capture capacity of both NaLTA and CaLTA is drastically reduced in the low-pressure range (see Figs. 3G and 3H), whereas it prevails at higher pressures (see Figs. 3G and 3I). By further increasing the temperature, the distance between the two isotherms drops, until their partial overlapping at 423 K, where NaLTA slightly overcomes the CaLTA capture capacity at 1000 mbar. The CO2 capture capacity decrease of LTA samples is especially evident at low pressures (100 mbar), where the CO$_2$ adsorption of CaLTA and NaLTA reduces of around 90 % and 87 % respectively, from 298 to 423 K. The adsorption behavior agrees with the literature data reporting the CO$_2$ adsorption capacity at low temperature of both 4 A and 5 A (mix of sodium and calcium) zeolites in comparison with 13 × zeolite [72–74].

The pristine Clino sample always exhibits a higher CO$_2$ adsorption capacity (blue curves and histograms) compared to exchanged NaClino (grey curves and histograms) and CaClino (green curves and histograms) samples. In contrast to LTA zeolite, the ion exchange seems not to enhance the CO$_2$ uptake. It appears that the heterogenous mix of cations present in the pristine natural zeolite is responsible for a stronger

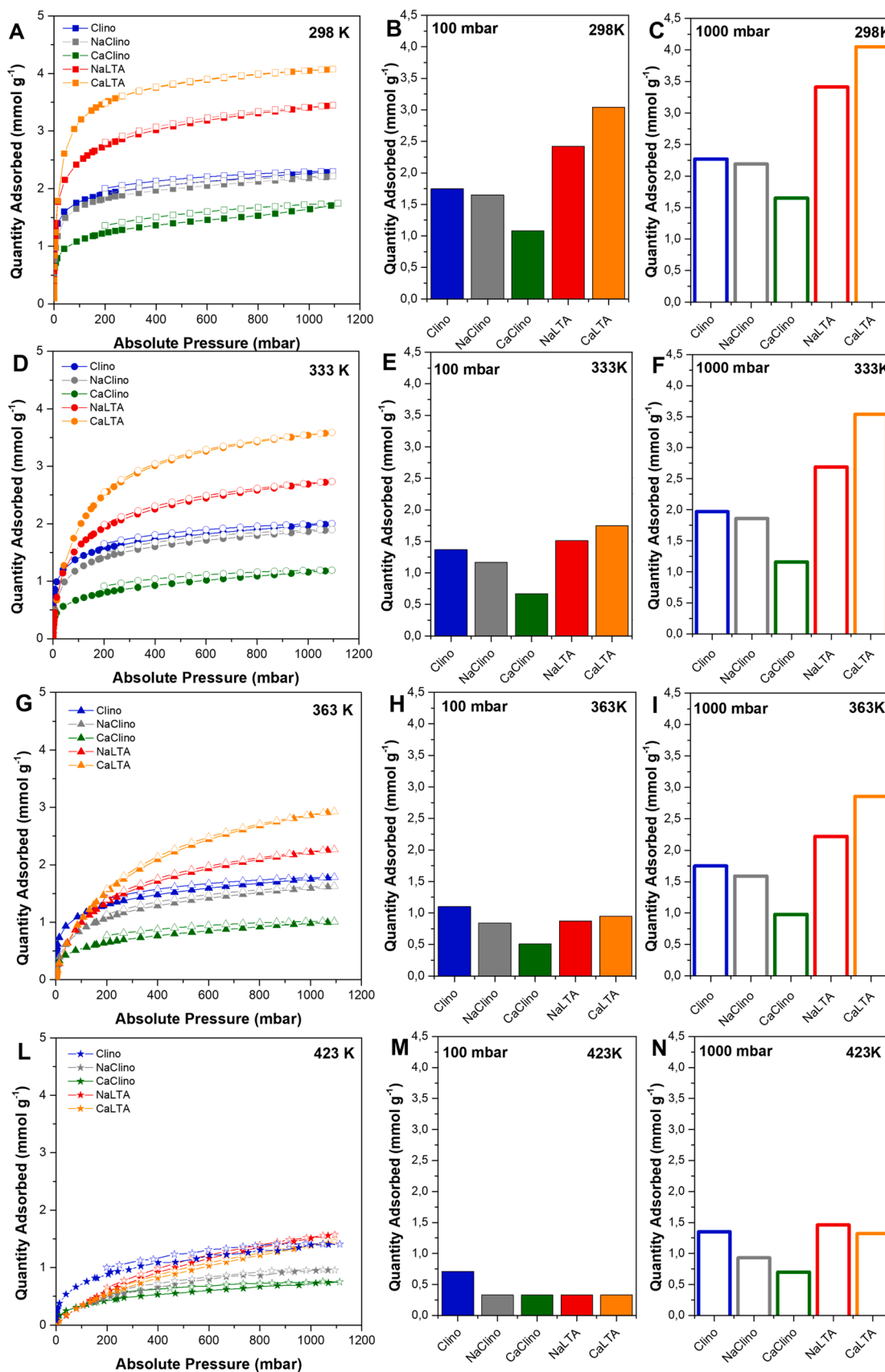**Fig. 3.** CO_2 adsorption/desorption isotherms at: A) 298, D) 333, G) 363 and L) 423 K. Quantity adsorbed in $mmol_{CO2}\ g^{-1}_{adsorbent}$ at 100 mbar absolute pressure at: B) 298, E) 333, H) 363 and M) 423 K. Quantity adsorbed in $mmol_{CO2}\ g^{-1}_{adsorbent}$ at 1000 mbar absolute pressure at: C) 298, F) 333, I) 363 and N) 423 K.

electrostatic interaction which leads to a higher CO_2 adsorption capacity compared to the exchanged samples [75]. This stronger interaction is preserved especially at higher temperatures (333 and 423 K), where the adsorption capacity of pure Clino in the low-pressure range overcomes the one of LTA. Moreover, at 423 K pristine Clino exhibits the best adsorption performances for nearly all the pressure range (until 800 mbar). The above reported results prove that pure Clino maintains a better CO_2 adsorption capacity at higher temperature compared to LTA samples, losing only the 61 % of its adsorption capacity at 100 mbar, by increasing the temperature from 298 to 423 K.

In general, at low temperature all the samples show a steep CO_2 uptake in the low-pressure region, whereas at higher temperature the adsorption capacity at the same pressure drastically decreases, except for pure Clino, which maintains discrete uptake capacity below 300 mbar. Moreover, both the exchanged Clino samples (NaClino and CaClino) show a reduced CO_2 adsorption at 423 K in the whole pressure range compared to raw Clino, proving that the CO_2 capture capacity at this temperature does not depend on the presence of Ca^{2+} or Na^+ ions, but it is probably related to the strong interaction with Fe^{2+} cations present only in the starting natural zeolite.

The CO_2 capture capacity of the materials was also investigated by performing a secondary adsorption run at 298 K, as explained in Section 5 of the SM, to study the reversibility of the adsorption process and evaluate the possible real use in cyclic adsorption/desorption experiments. The reversibility data clearly highlight that, although the ion-exchanged Clino samples do not exhibit enhanced CO_2 adsorption performances, they possess a higher CO_2 adsorption reversibility compared to raw Clino (see Fig. S4A–C and Table S2). The cyclic adsorption capacity is strictly related to the possible regeneration conditions of the material and, therefore, it must be considered for the use in real capture applications. For what concerns the LTA samples, the ion exchange procedure with Ca^{2+} affects the overall adsorption capacity at 298 K and, in parallel, provides a full reversibility of the material (see Fig. S4D and S4E).

The isosteric heat of adsorption was evaluated for the samples with the best CO_2 adsorption performances at 1000 mbar (i.e. NaLTA, CaLTA and Clino), by applying Eq. 1 on the isotherms collected at 298, 333 and 363 K, in the 0.2–2 mmol g^{-1} range of quantity adsorbed (Fig. 4). The isosteric heat value at vanishing coverage was extrapolated by considering the y-axis intercept and is reported in Table S3 (Section S6 of SI).

This isosteric heat of adsorption (Q_{st}), also reported as the opposite of the isosteric enthalpy of adsorption ($-\Delta H_{ads}$), is the heat released when
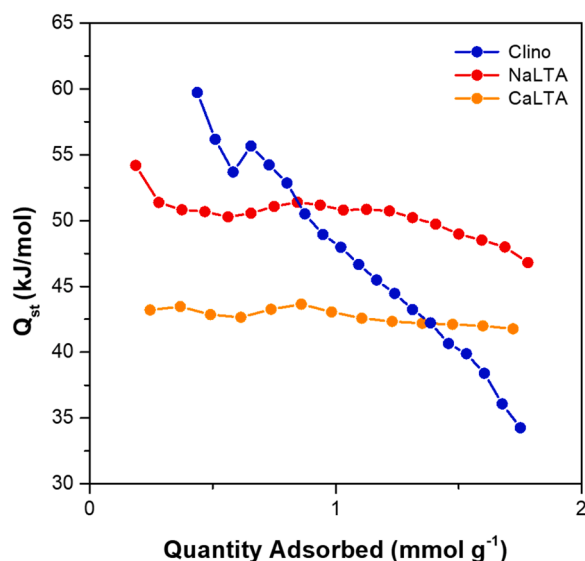
an adsorptive molecule interacts with a surface site [76]. The Q_{st} curves of NaLTA and CaLTA (see red and orange curves in Fig. 4) show a quite flat and constant trend, between 54 and 50 kJ/mol and 44–40 kJ/mol respectively. The lower isosteric heat of CaLTA sample testifies the weaker interaction between CO_2 and the Ca^{2+} cations compared to Na^+, fully compatible with the total reversibility displayed by this material upon a secondary CO_2 adsorption (Fig. S4E).

The isosteric heat of CO_2 adsorption of Clino is clearly distributed in a broader range, from 60 to 35 kJ/mol, confirming the great heterogeneity of cations present in the microchannels of the HEU framework, as already pointed out by EDX analysis and IR spectroscopy.

3.3. Evaluation of CO_2 adsorption capacity: breakthrough measurements

All the previously reported data were collected with pure CO_2 in static environment. However, the possible applications of those materials as adsorbents rarely require capture in static conditions. For this reason, breakthrough experiments under CO_2 flow were also performed. The results are shown in Fig. 5, where the CO_2 adsorption capacities of the materials at different temperatures (298, 333, 363 and 423 K, i.e., the same temperatures employed for the static experiments with pure CO_2) are reported as a function of time. The breakthrough curves are compared with the "blank" test, namely the reactor without the adsorbent material. As expected, by increasing the temperatures, the adsorption capacities decrease causing a shift of the breakthrough curves to shorter times.

Fig. 5A reports the breakthrough curves, along with the corresponding adsorption capacity (Fig. 5B) obtained at 298 K. The samples with the best adsorption capacities are Na- and CaLTA, about 3.1 and 3.3 mmol g^{-1} respectively (see Table S4 for all the adsorption capacities). Noteworthy, pristine Clino exhibits better performances compared to CaClino. On the other hand, at 298 K, the sample exchanged with Na^+ (NaClino) shows a higher CO_2 adsorption capacity. These results are in fair agreement with our previous studies [77].

By comparing the breakthrough measurements with the volumetric isotherms at 100 mbar of pure CO_2, some differences in the computed amount of CO_2 adsorbed are detectable, even if the trend among samples at the different temperatures is substantially the same (see Table S1 in comparison with Table S4). The reason of such variations could be due to the different experimental set-up (one working under a $N_2–CO_2$ flow, the other one working under equilibrium conditions with pure CO_2).

In Fig. 5C and 5D, the CO_2 breakthrough curves and the computed adsorption capacities at 333 K are reported respectively. It is worth noting that the CO_2 adsorption capacity trend is very similar to the situation observed at 298 K. At 363 K, the trend is again similar (Figs. 5E and 5F), except for the NaClino sample which exhibits lower adsorption capacity compared to pristine Clino.

Furthermore, the CaLTA sample has an adsorption capacity decrease, from 293 to 363 K which is higher comparing to NaLTA. This result agrees with the CO_2 volumetric adsorption data.

Finally, the adsorption capacity of the samples was tested at 423 K, and the results are reported in Fig. 5G and 5F. At this temperature, the most efficient adsorbent is Clino, with an adsorption capacity of 0.7 mmol g^{-1}, which decreases of 66 % compared to 298 K. These results are totally in line with the volumetric data. Again, the Clino sample is less affected by the variation of the temperature during the CO_2 adsorption tests, thanks to the presence in its framework of a consistent number of Fe^{2+} cations, which play a key role in the capture process at high temperature.

The ability to maintain good CO_2 capture performances in the middle-high temperature range is not straightforward, especially in zeolites where the high temperature drastically affects the adsorption capacity. Adsorbents for Carbon Capture and Storage are usually classified according to their best working temperature (low, medium and high capture temperature). Activated carbon, zeolites and MOFs are the most studied materials for low temperature applications (T < 200 °C) while
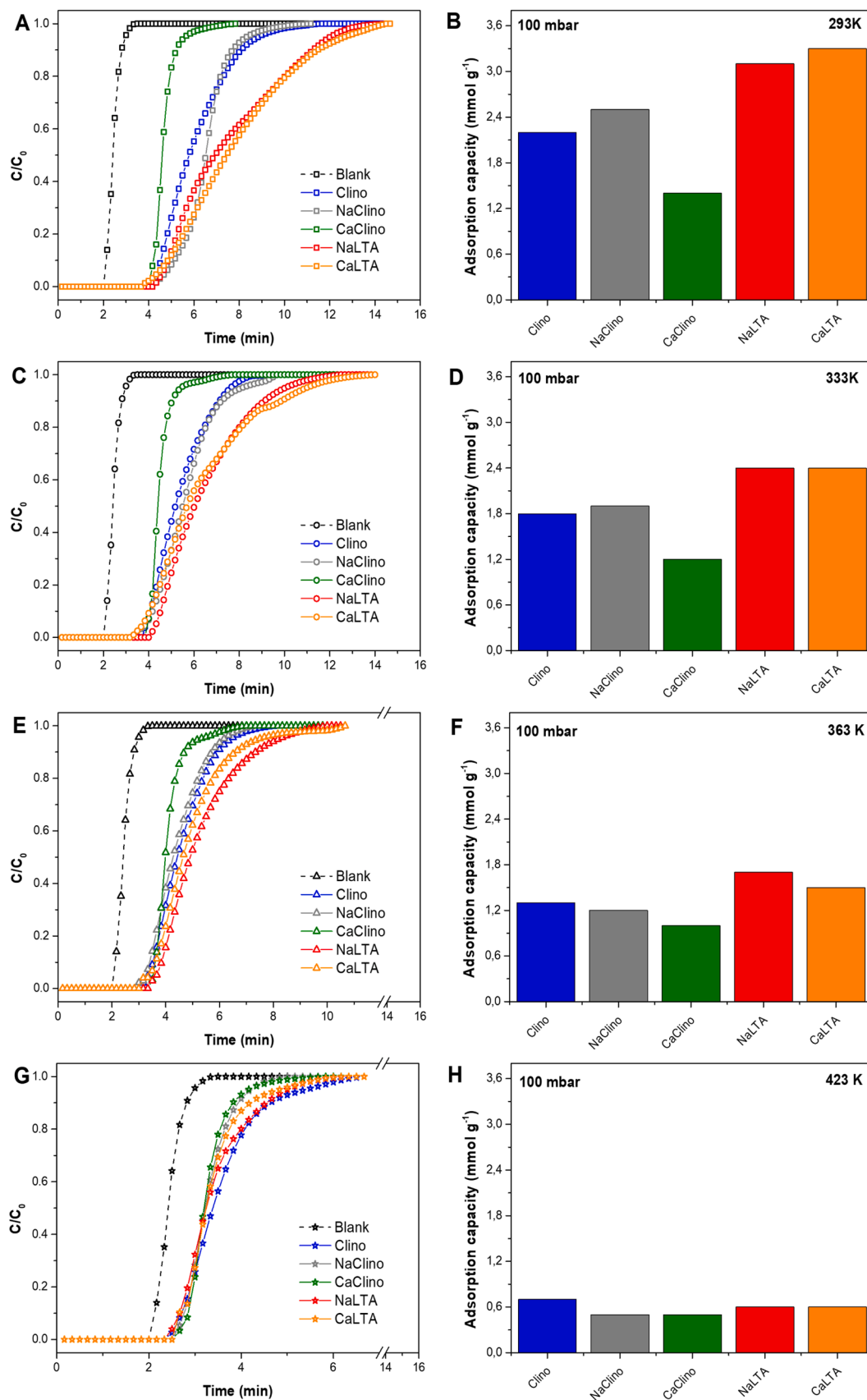

Fig. 4. Isosteric heat of CO_2 adsorption (Q_{st}) as a function of the quantity adsorbed, calculated from the isotherms at 298, 333 and 363 K.

Fig. 5. CO_2 breakthrough adsorption curves over the time at: A) 298, C) 333, E) 363 and G) 423 K. Computed adsorption capacity ($mmol_{CO2}\ g^{-1}_{adsorbent}$) at: B) 298, D) 333, F) 363 and H) 423 K.

hydrotalcites and oxides are usually applied for intermediate and high temperature applications respectively (200 < T < 400 °C and T > 400 °C) [78]. A comparison of those materials with LTA and Clino is reported in Table 3.

Activated carbons are low-cost materials easy to functionalize, displaying a good adsorption capacity at low temperature [85]. On the other hand, the shaping of this adsorbents is not simple and, moreover, they usually have low CO_2 selectivity and show a drop in the CO_2 capture capacity by increasing the adsorption temperature [79,80]. MOFs generally exhibit a higher CO_2 adsorption capacity compared to carbons and zeolites, together with a good selectivity and an easy tunability of the structure [86]. However, few MOFs maintain the same CO_2 capture performances when the temperature increases and most of them are sensitive to water [81]. Additionally, their scale up and shaping can be problematic. For this reason, zeolites seem to be more versatile than other microporous materials, and a lot of literature reports their application as possible carbon capture adsorbents [13]. In particular, 13 × is usually considered a reference zeolite for CO_2 capture. Certainly, its adsorption capacity is much higher than the other zeolitic framework, but the drop in performances by increasing the adsorption temperature is steeper compared to LTA and natural Clino [82].

Similarly to what described for low temperature materials, also hydrotalcites, which are usually employed for capture at intermediate temperature, show uncompetitive adsorption capacity at lower temperature [84]. Finally, for high temperature applications, different types of oxide are usually employed. In this case, a direct comparison with the previously mentioned materials is difficult, because the CO_2 capture can be considered as a high temperature absorption process [87].

Beside the excellent CO_2 uptake performances at medium-high temperature and the fair CO_2 capture capacity at low T, natural Clino has also a low commercial value compared to both LTA and 13X zeolites. Indeed, making an evaluation of the middle selling price of the three zeolites, an average cost for the capture of 1 kg of pure CO_2 can be computed, as reported in Table 4. This remark is particularly relevant if the adsorbents have to be used for large scale CO_2 capture.

Table 3

Comparison of CO_2 uptake capacities in the 298–673 K temperature range and 1 bar for different adsorbents.

Sample	Capture temperature (K)	CO_2 uptake at 1 bar (mmol$_{CO_2}$ g$^{-1}_{adsorbent}$)	Ref.
Activated Carbons	298	0.32–1.9	[79]
	348	0.2–1.7	[79]
	393	0.09–0.5	[80]
	423	–	–
CPO-27-Ni	303	0.52	[81]
	313	0.41	
	353	0.20	
13X	298	4.7	[79]
	348	3.2	[79]
	393	1.57	[82]
	423	–	–
MCM-41[a]	323	0.33	[83]
	348	0.20	
	373	0.15	
Clinoptilolite	298	2.3	This work
	348	–	
	363	1.8	
	423	1.4	
CaLTA	298	4.1	This work
	348	–	
	363	2.9	
	423	1.3	
Hydrotalcite MG305070	323	1–1.4	
	473	0.6–0.9	[84]
	673	0.7–0.95	

[a] Results obtained through TGA measurements.

Table 4

Comparison of average costs to capture 1 kg of CO_2 for different zeolites.

	Sample		
	Clino	LTA	13 X
Average price ($ for Ton)[a]	300 $	1300 $	2500 $
Cost to capture 1 kg of CO_2[b]	3.02 $	8.64 $	12.08 $

[a] Average prices based on the prices per ton of material provided by large Asian suppliers.

[b] Cost calculated assuming pure CO_2 capture at 1000 mbar and 298 K.

4. Conclusions

In this work, the CO_2 capture performances of a synthetic (LTA) and a natural (Clinoptilolite) zeolite are deeply investigated by means of advanced characterization approach. The two zeolites were studied in raw form and after ion exchange with Na^+ and Ca^{2+}, with the aim to possibly enhance the CO_2 adsorption capacity. The success of the exchange procedure was proved by means of EDX analysis, while XRD patterns highlighted the preservation of the crystalline structure. IR spectroscopy was used to investigate the accessibility of the different ions present inside the microporous structure and the strength of their interaction with the adsorbates. The specific surface area of the materials, measured using both N_2 and CO_2, showed that CaLTA was the only accessible material for N_2 molecules, while all the other displayed a great selectivity towards CO_2. Their potential application as solid CO_2 adsorbents was investigated by collecting both pure CO_2 adsorption/desorption isotherms and breakthrough curves under a N_2/CO_2 flow in a wide range of temperature (298–423 K).

Both the isotherm and the breakthrough curves of the materials exhibit a similar trend in CO_2 capture capacity with small discrepancies due to the different experimental conditions.

The cations exchanged process have a different impact on the CO_2 adsorption performances of the two zeolites. Indeed, the Ca^{2+} exchanged LTA gains both in adsorption capacity and reversibility compared to the standard LTA in sodic form. In contrast, the Na- and the Ca- form of Clinoptilolite have a higher CO_2 reversibility, but do not display a significant increment of the CO_2 uptake. By performing IR experiments with specific probe molecules, it was demonstrated that the presence of a consistent number of Fe^{2+} ions in the framework of natural Clino was responsible for the capacity of this material to strongly interact with CO_2.

Concerning the capture capacity, NaLTA and CaLTA exhibit a higher CO_2 uptake at lower temperature (i.e. 298 and 333 K), whereas the CO_2 adsorption performances of natural Clino, thanks to the presence of Fe^{2+} cations, are interesting also at medium-high temperature, being the most performant material at 423 K. In particular, the CO_2 capture capacity of pure Clino decreases of only 65 % passing from 298 to 423 K, compared to the reduction of 90 % observed for the CaLTA sample in the same range of temperature.

An industrially feasible adsorbent suitable for carbon capture should meet different requirements, not only in terms of mere carbon dioxide absolute loading. A good compromise could be a material easy to shape, exhibiting cyclic adsorption capacity, capable to maintain good adsorption performances in a wide range of temperature with possibly low production costs and, above all, with low sensitivity/selectivity to water. The CO_2/H_2O competitiveness and/or the sensitivity to moisture are key issues for different potential CO_2 adsorbents, as zeolites or MOFs, which often require a H_2O pre-capture step. Unfortunately, a CO_2 adsorbent which meet all those requirements does not still exist, despite the wide availability of literature data on carbon capture materials.

Assuming to previously dehydrate the flue gas (possibly using the same materials, since LTA is well-known as an industrial desiccant), the zeolites reported in this work possess some important features for potential CO_2 capture applications: they exhibit good CO_2 adsorption performances and reversibility in a wide range of temperature and are

already available in shaped form. Therefore, natural Clinoptilolite, commercialized in rock fragments (ø 0.15 mm), could be a possible interesting candidate for CO_2 capture until 423 K, with an average cost of 3\$ per kg of captured CO_2.

CRediT authorship contribution statement

Margherita Cavallo: Conceptualization, Methodology, Validation, Investigation, Data curation, Writing – original draft, Visualization. **Melodj Dosa:** Methodology, Validation, Investigation, Data curation, Writing – original draft, Writing – review & editing. **Natale Gabriele Porcaro:** Conceptualization, Methodology, Validation, Investigation. **Francesca Bonino:** Conceptualization, Resources, Writing – review & editing, Visualization, Supervision. **Marco Piumetti:** Conceptualization, Resources, Writing – review & editing, Supervision, Project administration, Funding acquisition. **Valentina Crocellà**: Conceptualization, Resources, Validation, Investigation, Data curation, Writing – review & editing, Supervision, Project administration, Funding acquisition.

Declaration of Competing Interest

The authors declare that they have no known competing financial interests or personal relationships that could have appeared to influence the work reported in this paper.

Data Availability

Data will be made available on request.

Acknowledgment

Appendix A. Supporting information

Supplementary data associated with this article can be found in the online version at doi:10.1016/j.jcou.2022.102335.

References

[1] United States Environmental Protection Agency, Overview of Greenhouse Gases | Greenhouse Gas (GHG) Emissions | US EPA, Epa, 2019. ⟨https://www.epa.gov/ghgemissions/overview-greenhouse-gases⟩, (Accessed 11 October 2022).
[2] D.A. Lashof, D.R. Ahuja, Relative contributions of greenhouse gas emissions to global warming, Nature 344 (1990) 529–531, https://doi.org/10.1038/344529a0.
[3] S. Sjostrom, H. Krutka, Evaluation of solid sorbents as a retrofit technology for CO_2 capture, Fuel 89 (2010) 1298–1306, https://doi.org/10.1016/j.fuel.2009.11.019.
[4] D. Saha, Z. Bao, F. Jia, S. Deng, Adsorption of CO_2, CH_4, N_2O, and N_2 on MOF-5, MOF-177, and zeolite 5A, Environ. Sci. Technol. 44 (2010) 1820–1826, https://doi.org/10.1021/es9032309.
[5] M. Wang, A. Lawal, P. Stephenson, J. Sidders, C. Ramshaw, Post-combustion CO_2 capture with chemical absorption: a state-of-the-art review, Chem. Eng. Res. Des. 89 (2011) 1609–1624, https://doi.org/10.1016/j.cherd.2010.11.005.
[6] A.B. Rao, E.S. Rubin, A technical, economic, and environmental assessment of amine-based CO_2 capture technology for power plant greenhouse gas control, Environ. Sci. Technol. 36 (2002) 4467–4475, https://doi.org/10.1021/es0158861.
[7] M. Khraisheh, S. Mukherjee, A. Kumar, F. Al Momani, G. Walker, M.J. Zaworotko, An overview on trace CO_2 removal by advanced physisorbent materials, J. Environ. Manag. 255 (2020), https://doi.org/10.1016/j.jenvman.2019.109874.
[8] A. Aquino, E. Bonamente, C. Buratti, F. Cotana, B. Castellani, V. Paolini, F. Petracchini, Carbon dioxide removal with tuff: experimental measurement of adsorption properties and breakthrough modeling using CFD approach, Energy Procedia (2016) 392–399, https://doi.org/10.1016/j.egypro.2016.11.050.
[9] T.E. Rufford, S. Smart, G.C.Y. Watson, B.F. Graham, J. Boxall, J.C. Diniz da Costa, E.F. May, The removal of CO_2 and N_2 from natural gas: a review of conventional and emerging process technologies, J. Pet. Sci. Eng. 94–95 (2012) 123–154, https://doi.org/10.1016/j.petrol.2012.06.016.
[10] S. Sjostrom, H. Krutka, Evaluation of solid sorbents as a retrofit technology for CO_2 capture, Fuel 89 (2010) 1298–1306, https://doi.org/10.1016/j.fuel.2009.11.019.
[11] D. Saha, Z. Bao, F. Jia, S. Deng, Adsorption of CO_2, CH_4, N_2O, and N_2 on MOF-5, MOF-177, and zeolite 5A, Environ. Sci. Technol. 44 (2010) 1820–1826, https://doi.org/10.1021/es9032309.
[12] N. Gargiulo, F. Pepe, D. Caputo, CO_2 adsorption by functionalized nanoporous materials: a review, J. Nanosci. Nanotechnol. 14 (2014) 1811–1822, https://doi.org/10.1166/jnn.2014.8893.
[13] T.H. Bae, M.R. Hudson, J.A. Mason, W.L. Queen, J.J. Dutton, K. Sumida, K. J. Micklash, S.S. Kaye, C.M. Brown, J.R. Long, Evaluation of cation-exchanged zeolite adsorbents for post-combustion carbon dioxide capture, Energy Environ. Sci. 6 (2013) 128–138, https://doi.org/10.1039/c2ee23337a.
[14] F.O. Ochedi, Y. Liu, Y.G. Adewuyi, State-of-the-art review on capture of CO_2 using adsorbents prepared from waste materials, Process Saf. Environ. Prot. 139 (2020) 1–25, https://doi.org/10.1016/j.psep.2020.03.036.
[15] E. Davarpanah, M. Armandi, S. Hernández, D. Fino, R. Arletti, S. Bensaid, M. Piumetti, CO_2 capture on natural zeolite clinoptilolite: effect of temperature and role of the adsorption sites, J. Environ. Manag. 275 (2020), 111229, https://doi.org/10.1016/j.jenvman.2020.111229.
[16] R. Ben-Mansour, M.A. Habib, O.E. Bamidele, M. Basha, N.A.A. Qasem, A. Peedikakkal, T. Laoui, M. Ali, Carbon capture by physical adsorption: materials, experimental investigations and numerical modeling and simulations – a review, Appl. Energy 161 (2016) 225–255, https://doi.org/10.1016/j.apenergy.2015.10.011.
[17] F.A. Mumpton, La roca magica: uses of natural zeolites in agriculture and industry, Proc. Natl. Acad. Sci. USA 96 (1999) 3463–3470, https://doi.org/10.1073/pnas.96.7.3463.
[18] F. Mumpton, Clinoptilolite redefined, Am. Miner. 45 (1960) 351–369.
[19] E.M. Flanigen, F.A. Mumpton, Commercial properties of natural zeolites, in: F. A. Mumpton (Ed.), Mineralogy and Geology of Natural Zeolites, De Gruyter, Berlin, Boston, 1977, pp. 165–176, https://doi.org/10.1515/9781501508585-012.
[20] G. Tsitsishvili, T. Andronikashvili, G. Kirov, L. Filizova, Nat. Zeolites (1992), https://doi.org/10.1163/_q3_SIM_00374.
[21] D.A. Kennedy, F.H. Tezel, Cation exchange modification of clinoptilolite – screening analysis for potential equilibrium and kinetic adsorption separations involving methane, nitrogen, and carbon dioxide, Microporous Mesoporous Mater. 262 (2018) 235–250, https://doi.org/10.1016/j.micromeso.2017.11.054.
[22] F. Collins, A. Rozhkovskaya, J.G. Outram, G.J. Millar, A critical review of waste resources, synthesis, and applications for zeolite LTA, Microporous Mesoporous Mater. 291 (2020), 109667, https://doi.org/10.1016/j.micromeso.2019.109667.
[23] E. Jaramillo, M. Chandross, N. Modine, Adsorption of small molecules in LTA-type zeolites: 1. NH_3, CO_2, and H_2O in zeolite 4A, Propos. Publ. J. Phys. Chem. B. 108 (2003) 20155–20159.
[24] D. Bonenfant, M. Kharoune, P. Niquette, M. Mimeault, R. Hausler, Advances in principal factors influencing carbon dioxide adsorption on zeolites, Sci. Technol. Adv. Mater. 9 (2008), https://doi.org/10.1088/1468-6996/9/1/013007.
[25] T.B. Reed, D.W. Breck, Crystalline zeolites. II. Crystal structure of synthetic zeolite, type A, J. Am. Chem. Soc. 78 (1956) 5972–5977, https://doi.org/10.1021/ja01604a002.
[26] D. Bonenfant, M. Kharoune, P. Niquette, M. Mimeault, R. Hausler, Advances in principal factors influencing carbon dioxide adsorption on zeolites, Sci. Technol. Adv. Mater. 9 (2008), https://doi.org/10.1088/1468-6996/9/1/013007.
[27] G. Li, P. Xiao, J. Zhang, P.A. Webley, D. Xu, The role of water on postcombustion CO_2 capture by vacuum swing adsorption: Bed layering and purge to feed ratio, AIChE J. 60 (2014) 673–689, https://doi.org/10.1002/aic.14281.
[28] M. Hefti, M. Mazzotti, Postcombustion CO_2 capture from wet flue gas by temperature swing adsorption, Ind. Eng. Chem. Res (2018), acs.iecr.8b03580, https://doi.org/10.1021/acs.iecr.8b03580.
[29] M. Hefti, L. Joss, Z. Bjelobrk, M. Mazzotti, On the potential of phase-change adsorbents for CO_2 capture by temperature swing adsorption, Faraday Discuss. 192 (2016) 153–179, https://doi.org/10.1039/C6FD00040A.
[30] F.P. Kinik, S. Kampouri, F.M. Ebrahim, B. Valizadeh, K.C. Stylianou, Porous metal-organic frameworks for advanced applications, in: Reference Module in Chemistry, Molecular Sciences and Chemical Engineering, Elsevier, 2020, https://doi.org/10.1016/B978-0-08-102688-5.00011-8.
[31] A. Farkaš, M. Rožić, Ž. Barbarić-Mikočević, Ammonium exchange in leakage waters of waste dumps using natural zeolite from the Krapina region, Croatia, J. Hazard. Mater. 117 (2005) 25–33, https://doi.org/10.1016/j.jhazmat.2004.05.035.
[32] Y.-F. Wang, F. Lin, W.-Q. Pang, Ammonium exchange in aqueous solution using Chinese natural clinoptilolite and modified zeolite, J. Hazard. Mater. 142 (2007) 160–164, https://doi.org/10.1016/j.jhazmat.2006.07.074.
[33] H. Valdés, S. Alejandro, C.A. Zaror, Natural zeolite reactivity towards ozone: the role of compensating cations, J. Hazard. Mater. 227–228 (2012) 34–40, https://doi.org/10.1016/j.jhazmat.2012.04.067.
[34] T.H. Bae, M.R. Hudson, J.A. Mason, W.L. Queen, J.J. Dutton, K. Sumida, K. J. Micklash, S.S. Kaye, C.M. Brown, J.R. Long, Evaluation of cation-exchanged zeolite adsorbents for post-combustion carbon dioxide capture, Energy Environ. Sci. 6 (2013) 128–138, https://doi.org/10.1039/c2ee23337a.
[35] V. Crocella, C. Atzori, G. Latini, M. Signorile, A Kit for PCT/IB2021/051769, Volumetric Measurements of Gas Adsorption, WO2021/181211A12021., n.d.
[36] M. Design, D. Group, A. Arbor, <Nature01650.Pdf>, 2003.

[37] A. Masala, F. Grifasi, C. Atzori, J.G. Vitillo, L. Mino, F. Bonino, M.R. Chierotti, S. Bordiga, CO$_2$ adsorption sites in UTSA-16: multitechnique approach, J. Phys. Chem. C 120 (2016) 12068–12074, https://doi.org/10.1021/acs.jpcc.6b03333.

[38] J.F. Marco, M. Gracia, J.R. Gancedo, T. González-Carreño, A. Arcoya, X.L. Seoane, On the state of iron in a clinoptilolite, Hyperfine Interact. 95 (1995) 53–70, https://doi.org/10.1007/BF02146305.

[39] K. Sato, Y. Nishimura, N. Matsubayashi, M. Imamura, H. Shimada, Structural changes of Y zeolites during ion exchange treatment: effects of Si/Al ratio of the starting NaY, Microporous Mesoporous Mater. 59 (2003) 133–146, https://doi.org/10.1016/S1387-1811(03)00305-6.

[40] L. Mihaly-Cozmuta, A. Mihaly-Cozmuta, A. Peter, C. Nicula, H. Tutu, D. Silipas, E. Indrea, Adsorption of heavy metal cations by Na-clinoptilolite: equilibrium and selectivity studies, J. Environ. Manag. 137 (2014) 69–80, https://doi.org/10.1016/j.jenvman.2014.02.007.

[41] N. Mansouri, N. Rikhtegar, H. Ahmad Panahi, F. Atabi, B.K. Shahraki, Porosity, characterization and structural properties of natural zeolite – clinoptilolite – as a sorbent, Environ. Prot. Eng. 39 (2013) 139–152, https://doi.org/10.5277/EPE130111.

[42] K. Menad, A. Feddag, K. Rubenis, Synthesis and study of calcination temperature influence on the change of structural properties of the LTA zeolite, Rasayan J. Chem. 9 (2016) 788–797.

[43] S. Bordiga, C. Lamberti, F. Bonino, A. Travert, F. Thibault-Starzyk, Probing zeolites by vibrational spectroscopies, Chem. Soc. Rev. 44 (2015) 7262–7341, https://doi.org/10.1039/c5cs00396b.

[44] K.I. Hadjiivanov, G.N. Vayssilov, Characterization of oxide surfaces and zeolites by carbon monoxide as an IR probe molecule, Adv. Catal. 47 (2002) 307–511, https://doi.org/10.1016/S0360-0564(02)47008-3.

[45] T. Montanari, I. Salla, G. Busca, Adsorption of CO on LTA zeolite adsorbents: an IR investigation, Microporous Mesoporous Mater. 109 (2008) 216–222, https://doi.org/10.1016/j.micromeso.2007.04.045.

[46] S. Bordiga, E. Garrone, C. Lamberti, A. Zecchina, C.O. Areán, V.B. Kazansky, L. M. Kustov, Comparative IR-spectroscopic study of low-temperature H2 and CO adsorption on Na zeolites, J. Chem. Soc. Faraday Trans. 90 (1994) 3365–3372, https://doi.org/10.1039/FT9949003367.

[47] M.W. Ackley, R.T. Yang, Diffusion in Ion = Exchanged CIinoptilolites, vol. 37, 1991, pp. 1645–56.

[48] L. Valenzano, B. Civalleri, S. Chavan, G.T. Palomino, C.O. Areán, S. Bordiga, Computational and experimental studies on the adsorption of CO, N$_2$, and CO$_2$ on Mg-MOF-74, J. Phys. Chem. C 114 (2010) 11185–11191, https://doi.org/10.1021/jp102574f.

[49] C. Otero Areán, G. Turnes Palomino, A. Zecchina, S. Bordiga, F.X. Llabrés, I. Xamena, C. Pazè, Vibrational spectroscopy of carbon monoxide and dinitrogen adsorbed on magnesium-exchanged ETS-10 molecular sieve, Catal. Lett. 66 (2000) 231–235, https://doi.org/10.1023/A:1019028513390.

[50] K. Hadjiivanov, E. Ivanova, H. Knözinger, FTIR study of low-temperature CO adsorption on Y zeolite exchanged with Be2+, Mg2+, Ca2+, Sr2+ and Ba2+ cations, Microporous Mesoporous Mater. 58 (2003) 225–236, https://doi.org/10.1016/S1387-1811(02)00650-9.

[51] M. Mihaylov, E. Ivanova, N. Drenchev, K. Hadjiivanov, Coordination chemistry of Fe^{2+} ions in Fe,H-ZSM-5 zeolite as revealed by the IR spectra of adsorbed CO and NO, J. Phys. Chem. C 114 (2010) 1004–1014, https://doi.org/10.1021/jp906213a.

[52] K. Hadjiivanov, FTIR study of low-temperature CO adsorption on Y zeolite exchanged with Be 2 Þ, Mg 2 Þ, Ca 2 Þ, Sr 2 Þ and Ba 2 Þ cations, vol. 58, 2003, pp. 225–36. ⟨https://doi.org/10.1016/S1387-1811(02)00650-9⟩.

[53] E. Garrone, R. Bula, K. Frolich, C.O. Area, M. Rodrı, P. Nachtigall, Single and dual cation sites in zeolites: theoretical calculations and FTIR spectroscopic studies on CO adsorption on K-FER, J. Phys. Chem. B 110 (2006) 22542–22550, https://doi.org/10.1021/jp0631331.

[54] K. Hadjiivanov, E. Ivanova, H. Knözinger, FTIR study of low-temperature CO adsorption on Y zeolite exchanged with Be2+, Mg2+, Ca2+, Sr2+ and Ba2+ cations, Microporous Mesoporous Mater. 58 (2003) 225–236, https://doi.org/10.1016/S1387-1811(02)00650-9.

[55] E. Garrone, R. Bula, K. Frolich, C.O. Area, M. Rodrı, P. Nachtigall, Single and Dual Cation Sites in Zeolites: Theoretical Calculations and FTIR Spectroscopic Studies on CO Adsorption on K-FER, 2006, pp. 22542–50.

[56] K. Hadjiivanov, E. Ivanova, H. Knözinger, FTIR study of low-temperature CO adsorption on Y zeolite exchanged with Be2+, Mg2+, Ca2+, Sr2+ and Ba2+ cations, Microporous Mesoporous Mater. 58 (2003) 225–236, https://doi.org/10.1016/S1387-1811(02)00650-9.

[57] C.O. Areán, M.R. Delgado, K. Frolich, R. Bulánek, A. Pulido, G.F. Bibiloni, P. Nachtigall, Computational and Fourier transform infrared spectroscopic studies on carbon monoxide adsorption on the zeolites Na-ZSM-5 and K-ZSM-5: evidence of dual-cation sites, J. Phys. Chem. C 112 (2008) 4658–4666, https://doi.org/10.1021/jp7109934.

[58] T. Montanari, I. Salla, G. Busca, Adsorption of CO on LTA zeolite adsorbents: an IR investigation, Microporous Mesoporous Mater. 109 (2008) 216–222, https://doi.org/10.1016/j.micromeso.2007.04.045.

[59] K.A. Cychosz, R. Guillet-Nicolas, J. García-Martínez, M. Thommes, Recent advances in the textural characterization of hierarchically structured nanoporous materials, Chem. Soc. Rev. 46 (2017) 389–414, https://doi.org/10.1039/C6CS00391E.

[60] K. Cho, H.S. Cho, L.C. De Ménorval, R. Ryoo, Generation of mesoporosity in LTA zeolites by organosilane surfactant for rapid molecular transport in catalytic application, Chem. Mater. 21 (2009) 5664–5673, https://doi.org/10.1021/cm902861y.

[61] Y.C. Feng, Y. Meng, F.X. Li, Z.P. Lv, J.W. Xue, Synthesis of mesoporous LTA zeolites with large BET areas, J. Porous Mater. 20 (2013) 465–471, https://doi.org/10.1007/s10934-012-9617-7.

[62] K. Cho, H.S. Cho, L.C. de Ménorval, R. Ryoo, Generation of mesoporosity in LTA zeolites by organosilane surfactant for rapid molecular transport in catalytic application, Chem. Mater. 21 (2009) 5664–5673, https://doi.org/10.1021/cm902861y.

[63] Zeolite Molecular Sieves: Structure, Chemistry, and Use D. W. Breck (Union Carbide Corporation, Tarrytown, New York) John Wiley and Sons, New York, London, Sydney, and Toronto, 1974. 771 pp. $11.95, J Chromatogr Sci. 13 (1975) 18A–18A. ⟨https://doi.org/10.1093/chromsci/13.4.18A-c⟩.

[64] A. Dziedzicka, B. Sulikowski, M. Ruggiero-Mikołajczyk, Catalytic and physicochemical properties of modified natural clinoptilolite, Catal. Today 259 (2016) 50–58, https://doi.org/10.1016/j.cattod.2015.04.039.

[65] Unger, K.K., Kreysa, G., Baselt, J.P. Studies in Surface Science and Catalysis, 2000.

[66] K.A. Cychosz, R. Guillet-Nicolas, J. García-Martínez, M. Thommes, Recent advances in the textural characterization of hierarchically structured nanoporous materials, Chem. Soc. Rev. 46 (2017) 389–414, https://doi.org/10.1039/c6cs00391e.

[67] J. Garcia-Martinez, D. Cazorla-Amoros, A. Linares-Solano, Further evidences of the usefulness of CO$_2$ adsorption to characterise microporous solids, Stud. Surf. Sci. 128 (2000) 485–494.

[68] M. Thommes, Textural characterization of zeolites and ordered mesoporous materials by physical adsorption, in: Stud Surf Sci Catal, Elsevier Inc., 2007, https://doi.org/10.1016/S0167-2991(07)80803-2.

[69] M. Thommes, K.A. Cychosz, Physical adsorption characterization of nanoporous materials: progress and challenges, Adsorption 20 (2014) 233–250, https://doi.org/10.1007/s10450-014-9606-z.

[70] N. Mehio, S. Dai, D. Jiang, Quantum mechanical basis for kinetic diameters of small gaseous molecules, J. Phys. Chem. A 118 (2014) 1150–1154, https://doi.org/10.1021/jp412588f.

[71] D. Lozano-Castelló, D. Cazorla-Amorós, A. Linares-Solano, Usefulness of CO$_2$ adsorption at 273 K for the characterization of porous carbons, Carbon (2004) 1233–1242, https://doi.org/10.1016/j.carbon.2004.01.037.

[72] Z. Liu, C.A. Grande, P. Li, J. Yu, A.E. Rodrigues, Adsorption and desorption of carbon dioxide and nitrogen on zeolite 5A, Sep Sci. Technol. 46 (2011) 434–451, https://doi.org/10.1080/01496395.2010.513360.

[73] S. Pakseresht, M. Kazemeini, M.M. Akbarnejad, Equilibrium isotherms for CO, CO$_2$, CH$_4$ and C$_2$H$_4$ on the 5A molecular sieve by a simple volumetric apparatus, Sep Purif. Technol. 28 (2002) 53–60, https://doi.org/10.1016/S1383-5866(02)00012-6.

[74] T.H. Bae, M.R. Hudson, J.A. Mason, W.L. Queen, J.J. Dutton, K. Sumida, K. J. Micklash, S.S. Kaye, C.M. Brown, J.R. Long, Evaluation of cation-exchanged zeolite adsorbents for post-combustion carbon dioxide capture, Energy Environ. Sci. 6 (2013) 128–138, https://doi.org/10.1039/c2ee23337a.

[75] D.A. Kennedy, M. Mujčin, C. Abou-Zeid, F.H. Tezel, Cation exchange modification of clinoptilolite –thermodynamic effects on adsorption separations of carbon dioxide, methane, and nitrogen, Microporous Mesoporous Mater. 274 (2019) 327–341, https://doi.org/10.1016/j.micromeso.2018.08.035.

[76] A. Nuhnen, C. Janiak, A practical guide to calculate the isosteric heat/enthalpy of adsorption: via adsorption isotherms in metal-organic frameworks, MOFs, Dalton Trans. 49 (2020) 10295–10307, https://doi.org/10.1039/d0dt01784a.

[77] E. Davarpanah, M. Armandi, S. Hernández, D. Fino, R. Arletti, S. Bensaid, M. Piumetti, CO$_2$ capture on natural zeolite clinoptilolite: effect of temperature and role of the adsorption sites, J. Environ. Manag. 275 (2020), 111229, https://doi.org/10.1016/j.jenvman.2020.111229.

[78] Q. Wang, J. Luo, Z. Zhong, A. Borgna, CO$_2$ capture by solid adsorbents and their applications: current status and new trends, Energy Environ. Sci. 4 (2011) 42–55, https://doi.org/10.1039/C0EE00064G.

[79] D.P. Bezerra, R.S. Oliveira, R.S. Vieira, C.L. Cavalcante, D.C.S. Azevedo, Adsorption of CO$_2$ on nitrogen-enriched activated carbon and zeolite 13X, Adsorption 17 (2011) 235–246, https://doi.org/10.1007/s10450-011-9320-z.

[80] M. Mercedes Maroto-Valer, Z. Lu, Y. Zhang, Z. Tang, Sorbents for CO$_2$ capture from high carbon fly ashes, Waste Manag. 28 (2008) 2320–2328, https://doi.org/10.1016/j.wasman.2007.10.012.

[81] P.D.C. Dietzel, R.E. Johnsen, H. Fjellvåg, S. Bordiga, E. Groppo, S. Chavan, R. Blom, Adsorption properties and structure of CO$_2$ adsorbed on open coordination sites of metal–organic framework Ni2(dhtp) from gas adsorption, IR spectroscopy and X-ray diffraction, Chem. Commun. (2008) 5125, https://doi.org/10.1039/b810574j.

[82] A. Lee, G. Xiao, P. Xiao, K. Joshi, R. Singh, P.A. Webley, High temperature adsorption materials and their performance for pre-combustion capture of carbon dioxide, Energy Procedia 4 (2011) 1199–1206, https://doi.org/10.1016/j.egypro.2011.01.174.

[83] X. Xu, C. Song, J.M. Andresen, B.G. Miller, A.W. Scaroni, Novel polyethylenimine-modified mesoporous molecular sieve of MCM-41 type as high-capacity adsorbent for CO$_2$ capture, Energy Fuels 16 (2002) 1463–1469, https://doi.org/10.1021/ef020058u.

[84] J.M. Lee, Y.J. Min, K.B. Lee, S.G. Jeon, J.G. Na, H.J. Ryu, Enhancement of CO$_2$ sorption uptake on hydrotalcite by impregnation with K$_2$CO$_3$, Langmuir 26 (2010) 18788–18797, https://doi.org/10.1021/la102974s.

[85] M. Mercedes Maroto-Valer, Z. Lu, Y. Zhang, Z. Tang, Sorbents for CO_2 capture from high carbon fly ashes, Waste Manag. 28 (2008) 2320–2328, https://doi.org/10.1016/j.wasman.2007.10.012.

[86] A. Samanta, A. Zhao, G.K.H. Shimizu, P. Sarkar, R. Gupta, Post-combustion CO_2 capture using solid sorbents: a review, Ind. Eng. Chem. Res. 51 (2012) 1438–1463, https://doi.org/10.1021/ie200686q.

[87] J.C. Abanades, E.J. Anthony, J. Wang, J.E. Oakey, Fluidized bed combustion systems integrating CO_2 capture with CaO, Environ. Sci. Technol. 39 (2005) 2861–2866, https://doi.org/10.1021/es0496221.